Adsorption Study of Surface and Structural Properties of MCM-41 Materials of Different Pore Sizes

M. Kruk and M. Jaroniec*

Department of Chemistry, Kent State University, Kent, Ohio 44242

A. Sayari

Department of Chemical Engineering and CERPIC, Universite Laval, Ste-Foy, Qc, Canada, G1K 7P4

Received: July 8, 1996; In Final Form: November 23, 1996[⊗]

Nitrogen adsorption measurements were performed over a wide range of relative pressures (10^{-6}−0.995) for a series of siliceous MCM-41 samples obtained using alkyltrimethylammonium surfactants with different chain length. Both high- and low-pressure adsorption data were analyzed. The pore size was shown to increase in a regular way with the chain length of the surfactant used. Moreover, a very good correlation between the pore size and the interplanar spacing of the MCM-41 samples was observed. Methods used to calculate the pore diameter were critically compared, and a new procedure to estimate the pore size of MCM-41 materials was proposed. This new procedure is based on geometrical considerations of the ratio of the pore volume to the pore wall volume for an infinite hexagonal array of cylindrical pores. Adsorption measurements showed that the amount adsorbed in the low-pressure region increases with a decrease in the pore size of the samples probably because of the enhancement of the gas−surface interactions caused by an increase in the curvature of pore walls. The adsorption energy distributions were found to be similar for all samples studied and quite close to those previously reported for porous silica gels. However, the adsorption energy distributions for the MCM-41 samples were exceptionally numerically stable.

1. Introduction

A considerable effort has been made to develop porous materials of well-defined pore geometry. Such materials are desirable as catalysts, catalyst supports, and shape/size selective adsorbents. Although the synthesis and application of ordered microporous solids, such as zeolites, have been well established,[1,2] numerous attempts to obtain geometrically regular mesoporous materials were unsuccessful until 1990, when Yanagisawa et al.[3] reported the synthesis of ordered mesoporous silicates by treatment of layered Kanemite silicates in the presence of alkyltrimethylammonium bromides (C*n*TAB). In 1991, researchers from Mobil Corporation used a liquid crystal templating approach to synthesize a large family of mesoporous silicates and aluminosilicates, currently known as the M41S molecular sieves.[4,5] Since then, this research area underwent a considerable growth. Progress in the synthesis, characterization, and potential applications of M41S materials was the subject of recent review papers.[6,7]

One of the members of the M41S family, namely, MCM-41, exhibits a hexagonal array of cylindrical pores whose diameter can be varied from 1.5 to 10 nm, depending on the preparation method. MCM-41 molecular sieves attract considerable and still growing attention because of their remarkable properties. They are easy to synthesize,[5] and their pore size can be tailored within a wide range by one of the following synthesis strategies: (i) the use of surfactants of appropriate chain lengths,[5] (ii) the addition of expander molecules such as trimethylbenzene,[5,8] and (iii) thermal restructuring.[9] Surface properties of MCM-41 materials can be modified by incorporating heteroatoms such as boron,[10,11] titanium,[12−14] vanadium,[15] and gallium.[16] Moreover, silanol groups present on the surface are suitable for chemical bonding of organic ligands[5,17] or anchoring inorganic species.[18,19] The ease of surface modification promises wide application of MCM-41 molecular sieves in the field of catalysis.[6,7]

From the very beginning, adsorption methods played a significant role in characterization of the new mesoporous materials.[4,5,20−29] The latter methods provide an easy and convenient way to probe surface properties and to calculate the specific surface area, the pore volume, and the pore size distribution of samples. It was soon recognized that MCM-41 opened up a unique opportunity for theoretical adsorption studies, serving as a model mesoporous solid.[25,26,28,29] Nitrogen adsorption results in the high-pressure range appeared to be especially interesting; namely, for samples with pores below 4 nm, a reversible, i.e., not accompanied by a hysteresis loop, pore-filling process was observed at the temperature of 77 K,[26,27] which had never been reported before for any mesoporous solid. This result apparently contradicts theoretical predictions[25] and therefore was the subject of nonlocal density functional[30] and computer simulation[31] studies, which showed that the hysteresis loop is expected to be present for monodisperse MCM-41 samples. It was suggested[31] that the absence of the hysteresis loop may possibly be attributed to pore size heterogeneity of MCM-41 samples.

Although high-pressure adsorption data for MCM-41 mesoporous materials were examined carefully,[4,5,16,17,20−29] to our best knowledge, low-pressure adsorption measurement results have not yet been published. In the current work, nitrogen adsorption measurements in a wide range of pressures (from 10^{-6} to 0.995 p/p_0) were carried out for a series of siliceous MCM-41 samples with pore sizes in the range from about 2 to 3.5 nm. Both low-pressure and high-pressure adsorption behaviors of the samples were examined and compared. In addition, various methods of the pore size calculation were

* To whom correspondence should be addressed. E-mail: Jaroniec@kentvm.kent.edu. Phone: (330) 672 3790. Fax: (330) 672 3816.

⊗ Abstract published in *Advance ACS Abstracts,* January 1, 1997.

S1089-5647(96)02000-7 CCC: $14.00

critically reviewed. Finally, the distributions of the adsorption energy for nitrogen were reported.

2. Materials and Methods

2.1. Materials. A series of MCM-41 silicates were synthesized hydrothermally as described earlier.[11] Alkyltrimethylammonium bromide (ATAB) surfactants with chain lengths of 8, 10, 12, 14, and 16 carbon atoms were used. A typical synthesis using cetyltrimethylammonium bromide (CTAB) was as follows. A mixture of 5 g of Cab-O-Sil M5 silica and 32.2 g of water was stirred vigorously for 10 min before a solution of 16.2 g of CTAB in 108.8 g of water was added. After an additional 10 min of stirring, a solution consisting of 14.36 g of tetramethylammonium silicate (10 wt % SiO_2) and 6.82 g of sodium silicate (28 wt % SiO_2, 10 wt % Na_2O) was added. The mixture was aged for 30 min under stirring, then transferred into a Teflon-lined autoclave and heated under autogenous pressure at 373 K for 24 h with no stirring. Then the sample was filtered, washed with deionized water, and dried in static air at 373 K. The calcination was carried out in two steps. The material was first heated under flowing dry nitrogen to 773 K at a rate of 1 K min^{-1} and kept for 2 h when the latter temperature was reached. Then nitrogen was slowly switched to dry air and the sample was heated at 773 K for an additional period of 4 h. In the current paper, the samples will be referred to as C*n*-MCM-41 or simply C*n* materials, where *n* designates the number of carbon atoms in the surfactant alkyl chain.

2.2. Measurements. X-ray powder diffraction spectra were recorded on a Philips PW1010 and a Siemens D-5000 X-ray diffractometers using nickel-filtered Cu Kα radiation. Nitrogen adsorption−desorption isotherms were measured at 77 K for relative pressures from about 10^{-6} to 0.995 using an ASAP 2010 volumetric adsorption apparatus from Micromeritics (Norcross, GA). Before the analysis, the samples were degassed under vacuum (about 10^{-3} Torr) at 423 K for 2 h in the degas port of the adsorption analyzer.

2.3. Characterization Methods. The specific surface area of the samples was obtained on the basis of the standard Brunauer−Emmett−Teller method.[32] For most samples studied, the condensation of the adsorbate inside the pores occurred within the pressure range usually used in the BET method (0.05−0.3 p/p_0). Therefore, the pressure limits had to be adjusted depending on the pore size of the samples and were varied from 0.06−0.25 to 0.04−0.10 p/p_0. The *t*-plot method[33,34] was employed to assess the microporosity of the samples (the statistical film thickness *t* from about 0.3 to 0.4 nm) and the volume and surface area of the mesoporous structures characteristic of the MCM-41 materials (*t* from about 0.6 to 0.9 nm). The Harkins−Jura isotherm was used to represent the isotherm on a reference nonporous adsorbent.

The pore size distribution (PSD) was obtained by means of the Barrett−Joyner−Halenda method[35] from the adsorption and desorption data in the pore size range 1−300 nm. The BJH method has recently been shown to underestimate the size of pores.[30,36] Therefore, other methods were also employed in the current study to evaluate the pore size of ordered cylindrical pores characteristic of the MCM-41 samples. In the current paper, the latter pores will be referred to as primary mesopores whereas other mesopores will be called secondary mesopores.

One of the methods, which allow us to calculate the diameter of cylindrical pores, is based on the following simple relation between the surface area S_p and the pore volume V_p for cylindrical pores: $w = 4V_p/S_p$.[27] If there is no evidence of microporosity for a given sample, the surface area S_p and the volume V_p of primary mesopores can be obtained from the *t*-plot method on the basis of adsorption data for higher statistical thicknesses of the adsorbed film in the way described below. In the region of pressures corresponding to the film thickness from about 0.5 to 0.8 nm, the primary mesopores of the MCM-41 materials can be considered as completely filled with the adsorbate and a further increase in the adsorbed amount can be attributed to a multilayer adsorption on the external surface of the samples. Therefore, the application of a comparative plot in the film thickness interval mentioned above allows for the calculation of the external surface area S_{ex} from the slope of its linear part, while the intercept provides the volume V_p of the primary mesopores. The difference between the BET surface area S_{BET} and the external surface area S_{ex} gives the surface area of the primary mesopores S_p . It needs to be remarked that even after the condensation of nitrogen in primary mesopores takes place, the density of the adsorbate inside the latter pores is expected to increase to some extent with increasing pressure. This effect may lead to overestimation of the external surface area but is not likely to cause a significant relative error in the primary mesopore volume V_p and the primary mesopore surface area S_p.

Another method employed to calculate the pore diameter is based on a simple geometric relation between the specific pore volume and the pore size for an infinite array of cylindrical pores arranged in a hexagonal fashion. In this case, the pore diameter *w* can be obtained from the pore volume V_p and the lattice spacing *d* (obtained from X-ray diffraction data) in the following way:

$$w = cd\left(\frac{\rho V_p}{1 + \rho V_p}\right)^{1/2} \tag{1}$$

where $c = (8/(3^{1/2}\pi))^{1/2}$ and ρ is the density of pore walls. It is assumed that the density of the adsorbate inside the pore is equal to the density of the liquid adsorbate at 77.4 K. The density of the pore walls ρ was set to be equal to the density of amorphous silica (2.2 g/cm^3).[37] In order for eq 1 to be accurate, a given sample needs to be of a good quality (it should consist only of hexagonal arrays of cylindrical pores).

A theoretical relation between the capillary condensation pressure and the pore size for MCM-41 materials was recently obtained by means of nonlocal density functional theory.[30] The latter relation was also employed in the current study to assess the diameter of pores for our samples on the basis of the pressure of the inflection point on the capillary condensation steps, which appear on the adsorption isotherms.

An advanced numerical procedure based on the regularization method[38] was used to obtain the adsorption energy distribution functions. The procedure performs an inversion of the integral equation of adsorption with respect to the adsorption energy distribution. The latter integral equation has the following form:

$$\Theta_t(p) = \int_{\epsilon_{min}}^{\epsilon_{max}} \theta_l(p, \epsilon) F(\epsilon)\, d\epsilon \tag{2}$$

where ϵ denotes the adsorption energy, which assumes values from an interval (ϵ_{min}, ϵ_{max}). $F(\epsilon)$ is an adsorption energy distribution, $\theta_l(p, \epsilon)$ is a local adsorption isotherm as a function of the adsorption energy ϵ and pressure *p*. $\Theta_t(p)$ stands for the total relative adsorption in the submonolayer region and can be calculated from an experimental adsorption isotherm $V(p)$ according to the following equation:

$$\Theta_t(p) = V(p)/V_{BET} \quad \text{for} \quad V(p) < V_{BET} \tag{3}$$

where V_{BET} is the BET monolayer capacity.

TABLE 1: Interplanar Spacing, Distance between Pore Centers, and BET Surface Area for the MCM-41 Samples[a]

sample	d (nm)	a (nm)	S_{BET} (m^3/g)	p_{BET}/p_0
C16	3.87	4.47	1240	0.06−0.25
C14	3.39	3.92	1220	0.04−0.15
C12	3.34	3.86	1140	0.04−0.14
C10	3.05	3.52	1120	0.04−0.11
C8	2.83	3.27	760	0.04−0.10

[a] d: interplanar spacing. a: distance between pore centers ($a = 2/3^{1/2}d$). S_{BET}: BET specific surface area. p_{BET}/p_0: relative pressure range used in the BET method.

In the current study, a local adsorption behavior was represented by the Fowler−Guggenheim (FG) isotherm[39] (localized monolayer adsorption with lateral interactions). Both patchwise and random models of topography of adsorption sites were applied. In the case of the patchwise model, the local FG isotherm for a given patch characterized by the adsorption energy equal to ϵ assumes the form

$$\theta_l(p, \epsilon) = \frac{K_L p \exp(z\omega q\theta_l/(k_B T))}{1 + K_L p \exp(z\omega\theta_l/(k_B T))} \quad (4)$$

where k_B is the Boltzmann constant, T stands for absolute temperature, z denotes the number of nearest neighbors, and ω is the interaction energy between two nearest neighbors. K_L is a Langmuirian constant for adsorption sites of the energy ϵ:

$$K_L = K_L^0(T) \exp(\epsilon/(k_B T)) \quad (5)$$

The preexponential factor $K_L^0(T)$ can be expressed in terms of partition functions for an isolated molecule in the gas and surface phases. In the case of the random model, the FG local adsorption isotherm assumes the following form:

$$\theta_l(p, \epsilon) = \frac{K_L p \exp(z\omega\theta_l/(k_B T))}{1 + K_L p \exp(z\omega\theta_l/(k_B T))} \quad (6)$$

In the current study, the lateral interaction energy parameter $z\omega/k_B$ was set to 190 K.

3. Results and Discussion

X-ray diffraction patterns of all Cn MCM-41 samples are displayed in Figure 1. Consistent with previous studies, the main (100) peak shifts to lower diffraction angles as n increases. In addition, the quality of the samples, as estimated from the width of the main peak and the appearance of higher diffraction angle peaks, increases with the length of the surfactant chain.

Shown in Table 1 are interplanar spacings d and distances between pore centers a ($a = 2/3^{1/2}d$). The values of a are spread over the range 3.27−4.47 nm and monotonically increase with an increase in the chain length of the surfactant used during the synthesis. Except for the C14 sample, the introduction of the $-(CH_2)_2-$ group in the surfactant aliphatic chain causes a regular increase of about 0.25 nm in the distance between the pore centers (see Figure 2), which is in a good agreement with previously reported results.[5]

Nitrogen adsorption isotherms for the MCM-41 samples are shown in Figure 3. Except for the C8 material, all samples exhibit a pronounced step on their isotherms for relative pressures 0.16−0.34 (see Table 1), arising from the condensation of nitrogen inside the primary mesopores. The condensation step on the isotherms is steep, particularly for C12, C14, and C16 materials, yet not vertical as expected on the basis of nonlocal density functional theory calculations[30] and computer simulations[31] for monodisperse pores of MCM-41 materials. The absence of a vertical jump on the adsorption isotherms for MCM-41 was attributed[31] to a slight pore size heterogeneity of the samples. However, the theoretical studies[30,31] were performed under the assumption of surface homogeneity, whereas the actual surface of siliceous materials is strongly heterogeneous because of its noncrystalline character and the presence of different surface groups, such as silanols and siloxanes.[37,40,41] It was shown[42] that surface heterogeneity may influence the pore filling process in such a way that it proceeds via a continuous pore filling instead of a first-order capillary condensation. Moreover, slight effects of the pore geometry heterogeneity can also be expected, since cylindrical pores of MCM-41 materials are curved, as it was recently shown by means of transmission electron microscopy.[43] All the factors mentioned above may account for the absence of vertical steps and hysteresis loops on the isotherms for the MCM-41 materials studied. It needs to be noted that numerous nitrogen adsorption studies[34] performed at the temperature of 77 K showed that adsorption−desorption hysteresis loops do not appear at relative pressures below ca. 0.42. Such a behavior was attributed to instability of the liquid nitrogen meniscus,[34] which was already

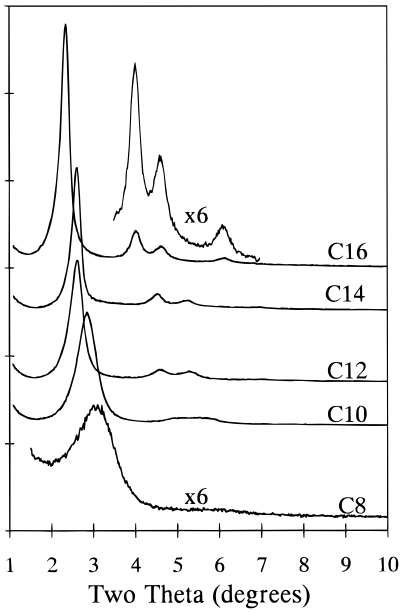

Figure 1. X-ray diffraction spectra for Cn MCM-41 samples. The values of n are shown on the right-hand side.

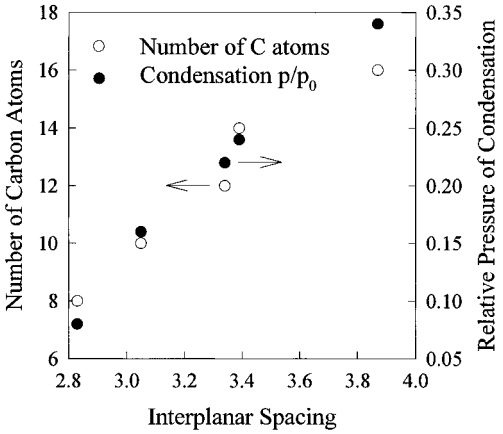

Figure 2. Relation between the interplanar spacing and the number of carbon atoms in the aliphatic chain of the surfactant used in the synthesis and between the interplanar spacing and the pressure of condensation in primary mesopores.

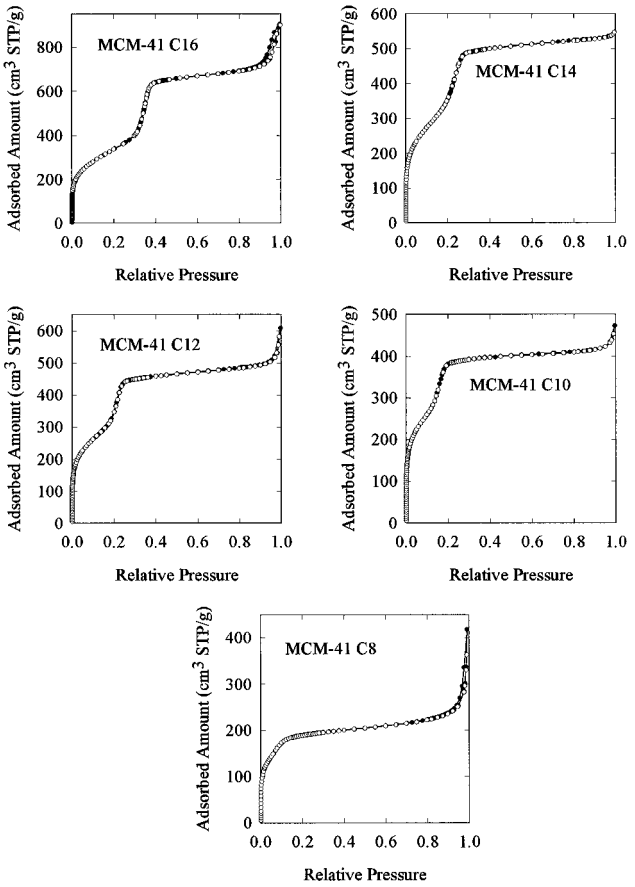

Figure 3. Nitrogen adsorption−desorption isotherms at 77 K.

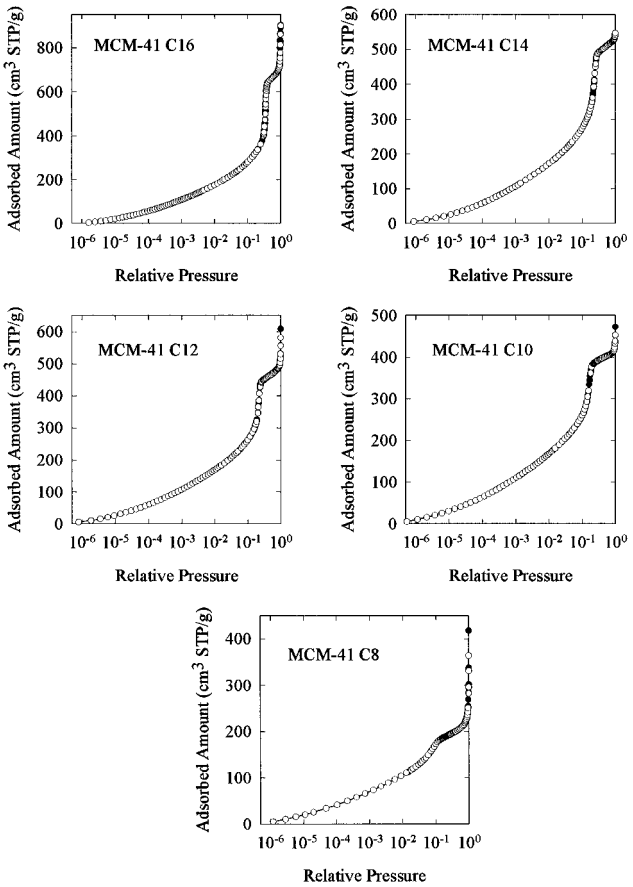

Figure 4. Adsorption isotherms at 77 K shown in a logarithmic scale.

suggested as an explanation of the reversible nitrogen condensation steps observed for MCM-41 materials.[26,28]

The relative pressure of the condensation in primary mesopores is well correlated with the interplanar spacing (see Figure 2). Note, for example, that the condensation pressures differ significantly for C16 and C14 but are very similar for C14 and C12 materials, which is in agreement with the magnitude of differences in their interplanar spacing (see Table 1). Because of the fact that the condensation pressure is related directly to the pore size (for samples with the same surface properties), these findings indicate that the pore size changes in a systematic way with the change in the interplanar spacing. Moreover, the above results suggest that the wall thickness does not change in an irregular way from one sample to another but either remains about constant or regularly changes with the interplanar spacing. This is in agreement with recent molecular dynamics computer simulations for MCM-41 materials,[44] which showed that in order for the porous structure to be stable, the wall thickness needs to increase to some extent when the distance between pore centers decreases.

In the case of the C8 MCM-41, the condensation step is not well-pronounced, but it is probably still present for the relative pressure of about 0.08. This can be seen more clearly on the isotherm in a logarithmic scale (see Figure 4). For all samples, the condensation step is reversible and there is no evidence of hysteresis, which is in agreement with previously reported data[26−29] for MCM-41 with a pore diameter below 4 nm. Some of the samples, especially C16 and C8 materials, exhibit a hysteresis loop in a higher-pressure region, which indicates the presence of a noticeable amount of secondary mesopores.

The primary mesopore volume of the samples studied decreases monotonously with the interplanar spacing (see Table 2), which indicates that the ratio of the primary mesopore volume to the volume of siliceous pore walls increases for materials with wider pores. The BET surface area is also higher for samples exhibiting a larger distance between pore centers. However, the primary mesopore surface area for C10−C16 materials does not vary in a systematic way, so the monotonic change in the S_{BET} is a coincidence resulting from a variable external surface area for the samples studied. It also needs to be realized that differences in the BET surface area S_{BET} and the primary mesopore surface area S_p are rather small and their analysis may be obscured by the inaccuracy of the methods used to calculate these quantities.

TABLE 2: Pore Volume, Surface Area, and Nitrogen Condensation Pressure for Primary Mesopores[a]

sample	V_p (cm^3/g)	S_p (m^2/g)	p_c/p_0
C16	0.91	1070	0.34
C14	0.70	1090	0.24
C12	0.63	1010	0.22
C10	0.57	1050	0.16
C8	0.26	680	0.08

[a] V_p and S_p: volume and surface area of primary mesopores. p_c/p_0: relative pressure of the inflection point corresponding to the condensation of nitrogen in primary mesopores.

The specific surface area of the samples was obtained from the BET method. The latter method needs to be applied with some caution because the condensation inside primary mesopores of MCM-41 materials may occur within a pressure range usually used in the BET analysis, e.g., 0.05−0.3 p/p_0. That was the case for most of the samples used in the current study. Shown in Figure 5 are BET plots for C16, C12, and C8 MCM-41 samples. In the case of the C16 material, a linear behavior was observed at least up to 0.25 p/p_0. However, the BET plot for the C12 sample shows strong deviations from linearity starting from a relative pressure of about 0.16, caused by the

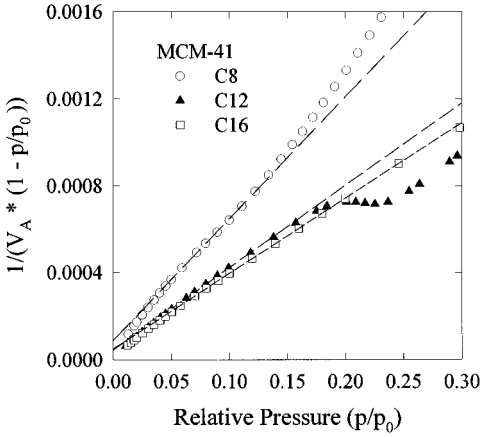

Figure 5. BET plots for selected MCM-41 samples.

condensation of nitrogen inside primary mesopores. Therefore, the pressure range used to obtain the BET surface area for the C12 material was appropriately narrowed (0.05−0.12 p/p_0) . In the case of the C8 sample, for which primary mesopores are filled at a relative pressure as low as ca. 0.08, it is difficult to choose a proper relative pressure interval to evaluate S_{BET} . The pressure range 0.04−0.1 may seem to be a good choice, since the BET fit obtained is rather good. However, when the latter interval was chosen, the obtained monolayer capacity was almost equal to a total volume of the primary mesopores V_p , as determined from the *t*-plot for a statistical film thickness from 0.5 to 0.8 nm. This result leads to the conclusion that the BET monolayer capacity and the BET surface area for the C8 material are considerably overestimated. This indicates that the BET method may be very inaccurate for MCM-41 samples with small pore sizes.

Shown in Figure 4 are isotherms in a logarithmic scale, which allows for better examination of the low-pressure adsorption properties of the samples. One can notice the similarity of the adsorption isotherms in the low-pressure region. The adsorbed amount increases gradually with increasing pressure and does not exhibit any steps until the pressure of condensation inside the primary mesopores is approached. At this point, a quite abrupt increase in the adsorbed amount takes place, except for the C8 sample, for which the latter step is not well-pronounced. The gradual increase in the gas uptake at low pressures (below the condensation pressure) resembles the low-pressure adsorption behavior of silica gels.[40,41] There is no pronounced step corresponding to a monolayer formation (such a step is noticeable for some other materials, for example, carbon blacks[45]) probably because of high surface heterogeneity.

To make a more accurate comparison of the low-pressure adsorption behavior of the samples studied, the isotherms were presented by plotting the degree of surface coverage vs the relative pressure of nitrogen. The degree of the surface coverage is defined as the amount adsorbed divided by the BET surface area of a given sample. Although the resulting curves are very similar in a relative pressure range from 5×10^{-7} to 5×10^{-2} (Figure 6), they exhibited an interesting behavior, which can be noticed especially in a pressure range from 5×10^{-7} to 10^{-3}. For all samples except the C8 material, the degree of surface coverage at a given pressure increases with the decrease in the pore size. This behavior can be explained in several ways. Most likely, the pore walls of smaller pores interact more strongly with the adsorbate because of their increased curvature. One can also expect some influence of the interaction potential of the opposite part of the pore wall, but this effect may be weak. Another possibility is that the number of strong interacting groups on the surface and maybe micropores (whose presence

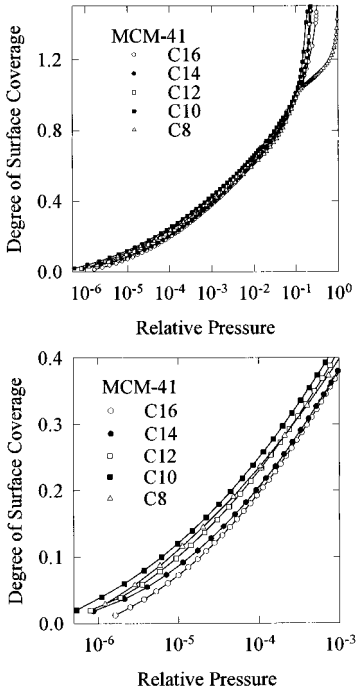

Figure 6. Comparison of adsorption behavior of the MCM-41 samples in a wide relative pressure range and the low-pressure range.

in small quantities is not evident but cannot be completely ruled out) increases as the size of MCM-41 primary mesopores decreases. Further studies are needed to thoroughly explain the observed enhancement in adsorption caused by the decrease in the pore size. As mentioned above, the C8 sample does not seem to exhibit the same low-pressure behavior as the other samples. This finding may result from an overestimation of its BET surface area. Hence, the surface coverage for the C8 sample may actually be greater than the surface coverage shown in Figure 6 and therefore in better agreement with the behavior observed for other samples.

The microporosity of the samples was estimated on the basis of the *t*-plot from adsorption data for pressures below the condensation pressure in primary mesopores. No evidence of the presence of microporosity was found. However, it needs to be remarked that an empirical Harkins−Jura adsorption isotherm was used to represent the isotherm for the reference nonporous material and therefore the *t*-plot results may be somewhat inaccurate.

Shown in Figure 7 are differential pore size distributions (PSDs) obtained from the BJH method on the basis of adsorption and desorption data for selected MCM-41 samples. Single sharp peaks on the PSDs can be noticed. Pore diameters corresponding to maxima of the peaks are listed in Table 3 as $w_{BJH\ ads}$ and $w_{BJH\ des}$. Pore diameters estimated on the basis of theoretical predictions[30] (nonlocal density functional theory) (w_{DFT}), primary mesopore volume and surface area ($w_{4V/S}$), and geometrical considerations (w_d) are also provided. The following trend was observed: $w_{DFT} > w_d > w_{4V/S} > w_{BJH\ des} > w_{BJH\ ads}$. This order is consistent with the fact that the BJH method was shown to underestimate the pore size.[30,36] It was also suggested[31] that the method based on the volume and surface area of primary mesopores[27] may lead to underestimation of the pore diameter, probably due to inaccuracy of the BET method employed. On the other hand, the evaluation of the pore diameter on the basis of the recent theoretical work[30] results in very low values of the pore wall thickness (see Table 4). The latter quantity was estimated on the basis of transmission electron microscopy to be about 1 nm.[20] Moreover, molecular dynamics simulation

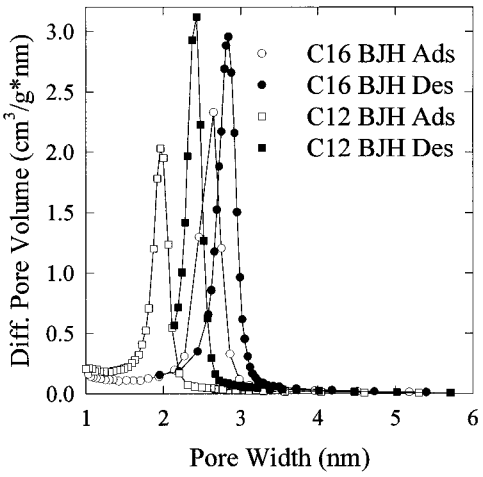

Figure 7. BJH differential pore size distributions obtained on the basis of nitrogen adsorption and desorption data for C12 and C16 samples.

TABLE 3: Comparison of Primary Mesopore Diameters Obtained by Different Calculation Methods[a]

sample	$w_{BJH\ ads}$	$w_{BJH\ des}$	w_{DFT}	$w_{4V/S}$	w_d
C16	2.70	2.84	4.0	3.40	3.82
C14	2.15	2.53	3.4	2.57	3.20
C12	2.07	2.43	3.2	2.50	3.09
C10	1.92		2.9	2.17	2.76
C8	1.32		2.4	1.53	2.07

[a] $w_{BJH\ ads}$ and $w_{BJH\ des}$: obtained from the maximum on the BJH pore size distribution calculated on the basis of adsorption (ads) and desorption (des) data. w_{DFT}: obtained on the basis of previously reported NL DFT calculations.[30] $w_{4V/S}$: calculated from the primary mesopore volume V_p and surface area S_p. w_d: calculated on the basis of the geometrical considerations.

TABLE 4: Comparison of Pore Wall Thicknesses Obtained by Different Calculation Methods[a]

sample	$b_{BJH\ ads}$	$b_{BJH\ des}$	b_{DFT}	$b_{4V/S}$	b_d
C16	1.77	1.63	0.5	1.07	0.65
C14	1.77	1.39	0.5	1.35	0.72
C12	1.79	1.43	0.7	1.36	0.77
C10	1.60		0.6	1.35	0.76
C8	1.95		0.9	1.74	1.20

[a] The pore wall thickness is denoted as *b*. Subscripts have the same meaning as those used in Table 3.

studies[44] showed that MCM-41 porous structures, which have a pore wall thickness less than 0.7 nm, are probably unstable and that their theoretical X-ray diffraction (XRD) patterns are not in agreement with experimental data. Simulated structures with pore walls equal to or greater than 1 nm gave rise to XRD patterns, which closely reproduced experimental results. It was also suggested that the pore size heterogeneity may bring XRD patterns for samples with somewhat smaller pore wall thicknesses (for example 0.8 nm) to agreement with experimental results. Therefore, the theoretical study[30] seems to underestimate the condensation pressure in pores of given sizes, which causes an overestimation of the pore size on the basis of experimental adsorption data. Further theoretical studies based on nonlocal density functional theory or computer simulation would be desirable to improve the accuracy of the relation between the pore size and the nitrogen condensation pressure for MCM-41 materials.

The method based on geometrical considerations of an infinite hexagonal array of cylindrical pores appears to give a quite reasonable estimation of the pore diameter, possibly overestimating them slightly. The pore diameters estimated on the basis of the latter method are shown in Figure 8. It is important that

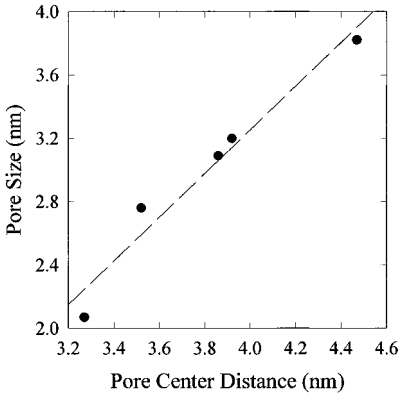

Figure 8. Relation between the pore size (calculated on the basis of X-ray interplanar spacing and the primary mesopore volume from *t*-plot) and the distance between pore centers.

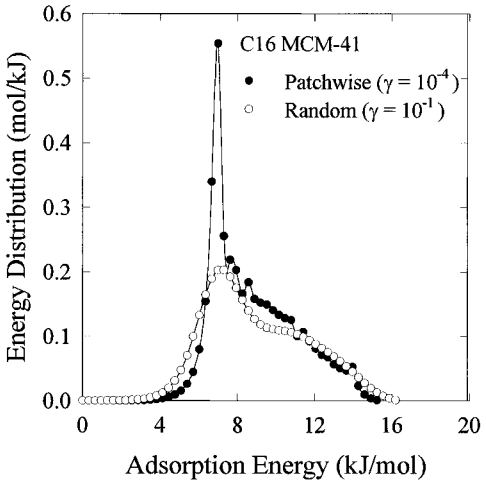

Figure 9. Adsorption energy distributions for the C16 sample calculated for random and patchwise topographies of adsorption sites.

the pore volume needed for the calculation may be obtained from adsorption data for adsorbates other than nitrogen or even from thermogravimetry.[46] However, the above method is expected to work properly for samples of excellent quality. In the case of lower quality samples (e.g., when the material is partially amorphous or comprised of very small particles), the primary mesopore size may be underestimated. There are also two other drawbacks of the method. The density of pore walls and the interplanar spacing from XRD need to be known. However, it should be recognized that in many cases, the application of this method to the evaluation of the pore diameter of MCM-41 samples seems to be quite convenient.

Shown in Figure 9 are adsorption energy distributions (AEDs) for the C16 MCM-41 sample. The AEDs for other samples are very similar, except for the C8 material. In the latter case, the differences may be caused mainly by inaccurate evaluation of the BET surface area. A sharp peak corresponding to the adsorption energy of about 7 kJ/mol can be noticed on the AED obtained under the assumption of the patchwise model. The position of the peak is somewhat dependent on the nearest neighbor interaction parameter $z\omega/k_B$ chosen for the calculations, but it is essentially independent of the choice of the regularization parameter γ, indicating a high numerical stability of the solutions for AEDs. Generally, the resulting AEDs are quite similar to the AEDs previously reported for silica gels[40,41] (some differences are mostly due to somewhat different nearest neighbor interaction parameters). However, the AEDs for MCM-41 exhibit exceptional numerical stability, even for

regularization parameters γ as low as $10^{-5}-10^{-8}$ for the patchwise topography of adsorption sites.

4. Conclusions

Nitrogen adsorption measurements over a wide pressure range allow for a detailed characterization of surface and structural properties of MCM-41 samples. Adsorption measurements can be used to assess the quality of MCM-41 materials on the basis of the steepness of the condensation step related to the primary mesopores as well as on the basis of the external surface area and the micropore volume obtained from the *t*-plot method. The pore size distribution and the primary mesopore diameter can also be calculated. However, there are some discrepancies between such results obtained by means of different methods. Therefore, a new method to calculate pore diameters for MCM-41 materials from adsorption (or thermal gravimetry) and X-ray diffraction data was proposed in the current study and shown to give quite reliable results.

In addition, low-pressure adsorption data were used to calculate adsorption energy distributions for the MCM-41 samples. To the best of our knowledge, the current work is the first paper reporting adsorption energy distributions for M41S materials. The samples under study exhibited a similar low-pressure adsorption behavior, which indicates their similar surface properties. However, it was shown that adsorption at the lowest accessible pressures (5×10^{-7} to 10^{-3} p/p_0) is noticeably enhanced by the decrease in the pore size. The latter result may be attributed to a slight increase in the gas−surface interaction energy caused by an increase in the pore wall curvature.

Acknowledgment. We are grateful to Ch. Danumah for preparation of the samples. A.S. thanks the Natural Sciences and Engineering Council of Canada (NSERC) for a partial support.

References and Notes

(1) *Introduction to Zeolite Science and Practice*; van Bekkum, H., Planigen, E. M., Jansen, J. C., Eds.; Elsevier: Amsterdam, 1988.
(2) *Advanced Zeolite Science and Applications*; Jansen, J. C., Stocker, M., Karge, H. G., Weitkamp, J., Eds.; Elsevier: Amsterdam, 1994.
(3) Yanagisawa, T.; Shimizu, T.; Kuroda, K.; Kato, C. *Bull. Chem. Soc. Jpn.* **1990**, *63*, 988, 1535.
(4) Kresge, C. T.; Leonowicz, M. E.; Roth, W. J.; Vartuli, J. C.; Beck, J. S. *Nature* **1992**, *359*, 710.
(5) Beck, J. S.; Vartuli, J. C.; Roth, W. J.; Leonowicz, M. E.; Kresge, C. T.; Schmitt, K. D.; Chu, C. T.-W.; Olson, D. H.; Sheppard, E. W.; McCullen, S. B.; Higgins, J. B.; Schlenker, J. L. *J. Am. Chem. Soc.* **1992**, *114*, 10834.
(6) Sayari, A. *Chem. Mater.* **1996**, *8*, 1840.
(7) Sayari, A. In *Recent Advances and New Horizons in Zeolite Science and Technology*; Chon, H., Woo, S. I., Park, S.-E., Eds.; Elsevier: Amsterdam, 1996; Chapter 1.
(8) Huo, Q.; Margolese, D. I.; Ciesla, U.; Feng, P.; Gier, T. E.; Sieger, P.; Leon, R.; Petroff, P. M.; Shüth, F.; Stucky, G. D. *Chem. Mater.* **1994**, *6*, 1176.
(9) Khushalani, D.; Kuperman, A.; Ozin, G. A.; Tanaka, K.; Garces, J.; Olken, J. J.; Coombs, N. *Adv. Mater.* **1995**, *7*, 842.
(10) Sayari, A.; Danumah, C.; Moudrakovski, I. L. *Chem. Mater.* **1995**, *7*, 813.
(11) Sayari, A.; Moudrakovski, I. L.; Danumah, C.; Ratcliffe, C. I.; Ripmeester, J. A.; Preston, K. F. *J. Phys. Chem.* **1995**, *99*, 16373.
(12) Corma, A.; Navarro, M. T.; Perez-Pariente, J. *J. Chem. Soc., Chem. Commun.* **1994**, 147.
(13) Tanev, P. T.; Chibwe, M.; Pinnavaia, T. J. *Nature* **1994**, *368*, 321.
(14) Sayari, A.; Reddy, K. M.; Moudrakovski, I. L. *Stud. Surf. Sci. Catal.* **1995**, *98*, 19.
(15) Reddy, K. M.; Moudrakovski, I. L.; Sayari, A. *J. Chem. Soc., Chem. Commun.* **1994**, 1059.
(16) Cheng, C.-F.; He, H.; Zhou, W.; Klinowski, J.; Goncalves, J. A. S.; Gladden, L. F. *J. Phys. Chem.* **1996**, *100*, 390.
(17) Brunel, D.; Caurel, A.; Fajula, F.; DiRenzo, F. *Stud. Surf. Sci. Catal.* **1995**, *97*, 173.
(18) Maschmeyer, T.; Rey, F.; Sankar, G.; Thomas, J. M. *Nature* **1995**, *378*, 159.
(19) Morey, M.; Davidson, A.; Eckert, H.; Stucky, G. D. *Chem. Mater.* **1996**, *8*, 486.
(20) Chen, C.-Y.; Li, H.-X.; Davis, M. E. *Microporous Mater.* **1993**, *2*, 17.
(21) Rathousky, J.; Zukal, A.; Franke, O.; Schulz-Ekloff, G. *J. Chem. Soc., Faraday Trans.* **1994**, *90*, 2821.
(22) Rathousky, J.; Zukal, A.; Franke, O.; Schulz-Ekloff, G. *J. Chem. Soc., Faraday Trans.* **1995**, *91*, 937.
(23) Llewellyn, P. L.; Schüth, F.; Grillet, Y.; Rouquerol, F.; Rouquerol, J.; Unger, K. K. *Langmuir* **1995**, *11*, 574.
(24) Tanev, P. T.; Pinnavaia, T. J. *Science* **1995**, *267*, 865.
(25) Schmidt, R.; Stöcker, M.; Hansen, E.; Akporiaye, D.; Ellestad, O. H. *Microporous Mater.* **1995**, *3*, 443.
(26) Branton, P. J.; Hall, P. G.; Sing, K. S. W. *J. Chem. Soc., Chem. Commun.* **1993**, 1257.
(27) Franke, O.; Schulz-Ekloff, G.; Rathousky, J.; Starek, J.; Zukal, A. *J. Chem. Soc., Chem. Commun.* **1993**, 724.
(28) Branton, P. J.; Hall, P. G.; Sing, K. S. W.; Reichert, H.; Schüth, F.; Unger, K. K. *J. Chem. Soc., Faraday Trans.* **1994**, *90*, 2965.
(29) Llewellyn, P. L.; Grillet, Y.; Schüth, F.; Reichert, H.; Unger, K. K. *Microporous Mater.* **1994**, *3*, 345.
(30) Ravikovitch, P. I.; Domhnaill, S. C. O.; Neimark, A. V.; Schüth, F.; Unger, K. K. *Langmuir* **1995**, *11*, 4765.
(31) Maddox, M. W.; Gubbins, K. E. *Int. J. Thermophys.* **1994**, *15*, 1115.
(32) Brunauer, S.; Emmett, P. H.; Teller, E. *J. Am. Chem. Soc.* **1938**, *60*, 309.
(33) Jaroniec, M. In *Access to Nanoporous Materials*; Pinnavaia, T. J., Thorpe, M. F., Eds.; Plenum Press: New York, 1996; p 255.
(34) Gregg, S. J.; Sing, K. S. W. *Adsorption, Surface Area and Porosity*; Academic Press: London, 1982.
(35) Barrett, E. P.; Joyner, L. G.; Halenda, P. P. *J. Am. Chem. Soc.* **1951**, *73*, 3, 373.
(36) Lastoskie, C.; Gubbins, K. E.; Quirke, N. *J. Phys. Chem.* **1993**, *97*, 4786.
(37) *The Colloid Chemistry of Silica*; Bergna, H. E., Ed.; American Chemical Society: Washington, DC, 1994.
(38) von Szombathely, M.; Brauer, P.; Jaroniec, M. *J. Comput. Chem.* **1992**, *13*, 17.
(39) Jaroniec, M.; Madey, R. *Physical Adsorption on Heterogeneous Solids*; Elsevier: Amsterdam, 1988.
(40) Bereznitski, Y.; Jaroniec, M.; Kruk, M. *J. Liq. Chromatogr.* **1996**, *19*, 1523.
(41) Bereznitski, Y.; Jaroniec, M.; Kruk, M.; Buszewski, B. *J. Liq. Chromatogr.* **1996**, *19*, 2767.
(42) Karykowski, K.; Rzysko, W.; Patrykiejew, A.; Sokolowski, S. *Thin Solid Films* **1994**, *249*, 236.
(43) Chenite, A.; Le Page, Y.; Sayari, A. *Chem. Mater.* **1995**, *7*, 1015.
(44) Feuston, B. P.; Higgins, J. B. *J. Phys. Chem.* **1994**, *98*, 4459.
(45) Kruk, M.; Jaroniec, M.; Bereznitski, Y. *J. Colloid Interface Sci.* **1996**, *182*, 282.
(46) Jaroniec, J.; Gilpin, R. K.; Rambler, J.; Choma, J. *Thermochim. Acta* **1996**, *272*, 65.